SAND2014-18452C

Evaluation Method for Arc Fault Detection Algorithms

Stephen McConnell[1], Zhan Wang[1], Robert S. Balog[1], and Jay Johnson[2]

[1]Texas A&M University, College Station, Texas, 77840, USA

[2]Sandia National Laboratories, Albuquerque, New Mexico, 87185, USA

***Abstract* — Many methods have been proposed to detect arc faults within photovoltaic systems. However, because of the dearth of data surrounding arcs that actually occur in commercial or residential PV systems, a sound method is necessary to systematically check for the effectiveness of algorithms claiming the ability to detect PV arc faults. This method should include data representing actual background PV system noise and seek to quantify the limits of the detection capability for the algorithms of interest.**

***Index Terms* — arc discharges, detection algorithms, photovoltaic systems.**

I. Introduction

Changes in the National Electrical Code® (2011) and the UL 1699B safety standard call for the ubiquitous use of arc fault detectors in photovoltaic arrays [1]. Without these devices, solar arrays remain vulnerable to the risk of fire hazard, which can hamper the widespread adoption of renewable energy resources.

Research applicable to photovoltaic arc fault detection tends to focus around experimental case studies of arcing scenarios. These scenarios include parallel and series arcs [1, 2], and arcs fabricated through diverse mechanisms, e.g., pull-apart method, steel-wool, etc. Many have proposed methods for detecting such arcs including those involving Fourier frequency band analysis, time-domain amplitude monitoring, and even analysis of electric field strength dynamics through electromagnetic sensors [3, 4].

What many of these attempts lack is a method to test the robustness of their proposed detection schemes. The data incorporated for detection benchmarking may be produced by carefully controlled experiment, but is it effective in representing a host of real-world PV systems?

Every solar array tied to the grid contains an electric-noise-producing solar inverter, and each brand or model of inverter carries its own background noise waveforms. The diversity and the potency of this background noise require that arc-detection methods must be able to distinguish between it and the erratic behavior associated with the actual occurrence of an arc fault. Because of this need, the authors propose a technique of embedding known arc signatures within a large dataset of inverter noise recordings in order to test the efficacy of the various detection methodologies. Once a digital library has been created, inverter noise and arc signals can be combined at different ratios and replayed for specified durations in order to test the robustness of digital detection algorithms. We introduce the relevant ASNR parameter for signal synthesis.

This proposal operates under the assumption that regardless of the source of the signals, e.g., voltage or current measurements from cables or sensors that are used to observe the surrounding circuitry or environment of an arc, it is feasible to sample these signals and implement a digital algorithm for detection.

II. Constructing a Dataset

The authors collected and compiled a data bank of inverter current noise signatures, each in length approximately 1/20th of a second. Though a good step in the right direction, these noise clips fall short of a desirable time duration for testing. An effective arc detection algorithm must not only unfailingly detect the presence of an arc but also must not nuisance trip or give false positives during signal input that contains only background noise. In order to thoroughly test both equally significant capacities, we desire a signal 1-10 seconds in duration.

A. Approach

An approach to solve the inadequate signal length problem which seems straightforward is to take an FFT of a given signal to obtain the frequency spectrum and then use an inverse FFT to recreate an extended time-domain waveform. However, this approach does not come without its challenges.

The traditional inverse DTFT is defined as follows [5]:

$$x[n] = \frac{1}{2\pi}\int_{-\pi}^{\pi} X(e^{j\omega})e^{j\omega n}d\omega \qquad (1)$$

where

$$X(e^{j\omega}) = \sum_{n=-\infty}^{\infty} x[n]e^{-j\omega n} \qquad (2)$$

(1) is often termed the synthesis equation with the DTFT in (2) below it comparatively referred to as the analysis equation. These two equations form a reversible set of point-to-point calculations with a frequency resolution equal to the sampling rate divided by the signal length, *N*. In other words, the differential, $d\omega$, in (1) is limited to increments of the frequency resolution for finite, discrete-time computations. Consequently, while the efficient IFFT algorithm can reproduce exactly the original time-domain signal associated with the spectral result of the FFT, it cannot exceed the

resolution of the FFT result which is determined only by the sampling rate and number of samples in the original signal.

Our implementation is similar to IFFT, but differs according to the following formula:

$$x[n] = \sum_{m=0}^{\frac{NFFT}{2}} X[m] \cos\left(2\pi \frac{m \cdot n}{N} + \varphi[m]\right) \qquad (3)$$

where X[m] and $\varphi[m]$ are the magnitude and phase of the FFT result at increments of the frequency resolution. Note that we use $NFFT/2$ because we build our reconstructed signal from the half-spectrum of the symmetric FFT result. We also scale our FFT result to compensate for the $1/2\pi$ term present in the synthesis equation during reconstruction.

B. Signal Extension Challenges

When working in conjunction with the FFT, our method as well as the IFFT encounters additional complications in the specific task of time-domain signal extension. The FFT requires that its parameter of both signal and spectral length, *NFFT*, must be a power of two in order to maximize the efficiency of computations. If $\log_2 N$ is not a positive integer, then the original signal is zero-padded in order to make it conform to this power-of-two length requirement. While such zero-padding has no adverse effect on the accuracy of the spectral result of the FFT, it does pose a problem in recreating the time-domain signal. Specifically, when the signal is reconstructed for a time interval exceeding the original signal length, *N*, the zero-padded segment will re-emerge as part of the recreated signal.

Fig. 1 illustrates this behavior. A 1MHz inverter noise signal containing 52,429 points is zero-padded to the next power of two: 65,536 (2^{16}) points. The mean or DC offset is then subtracted for analytical convenience. After extending the signal to an approximate ¼ second duration using FFT and subsequent IFFT-based reconstruction, multiple intervals of zero-valued signal appear.

The number of blank intervals that appear in a time-extended signal is predictable by the ratio of the final time-domain signal length to the length of the finite FFT spectral result. Specifically, for any real scalar multiple, k, the number of complete intervals, b_k, embedded within the extended signal is given by

$$b_k = \left\lfloor \frac{k * N}{NFFT} \right\rfloor \qquad (4)$$

In the example of Fig. 1, k = 5.5, and the corresponding number of intervals is 4 as expected.

Another problem with using an IFFT-based method of time-domain signal extension is that reconstruction past the original signal length—when $n > N$-1 in (3)—relies on periodic extension. For any particular frequency component, rather than creating a smooth extension of that component for $n > N$-1, periodic extension means restarting the component at $n = N$ with the same magnitude and phase attributes that it had at $n = 0$. This "replay" effect is carried out on all frequency components in the spectrum. Consequently, the frequency content of the reconstructed signal will not be consistent at integer multiples of the signal length. Inconsistent frequency content could easily be a source of error for arc detection algorithms.

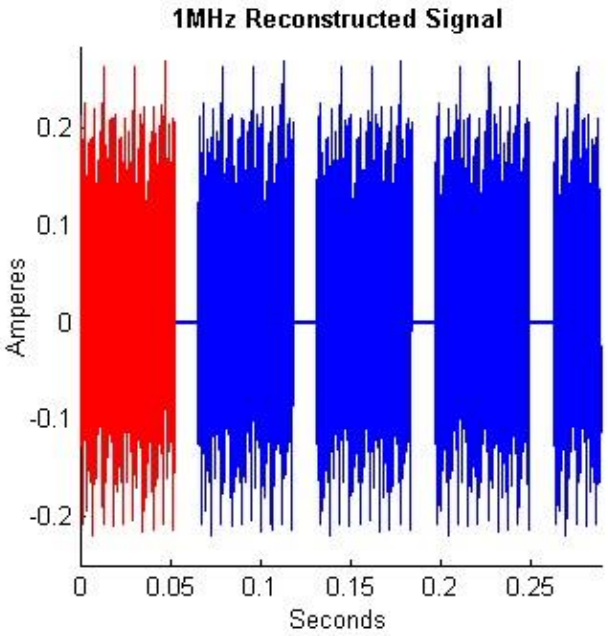

Fig. 1. The original inverter noise waveform (red) is extended to a time interval 5.5 times its original length (blue) using IFFT-based reconstruction.

C. Proposed Signal Extension Solutions

The zero-valued segments in the reconstructed signal can be minimized by eliminating the zero-padding of the original signal. In other words, we must choose a base signal of length N such that $\log_2 N$ is a positive integer. In the case of the 1MHz inverter noise signal, we could select a subset of contiguous points from the original sampled signal in length corresponding to the next largest power of two less than *N*, but that also involves a reduction in the resolution of our reconstruction result by a factor of two.

Instead, using a background noise signal of equivalent time duration from the same inverter that is sampled at a rate of 5MHz, we start with 262144 (2^{18}) points. Now that no zero-padding is required before performing the FFT on the 5MHz signal, the signal produced from reconstruction has no readily observable breaks or blank intervals (see Fig. 2).

To ensure the quality of the reconstruction method, the spectrum of the original signal and the reconstructed signal can be scrutinized with frequency analysis tools. Fig. 3 shows the result of a discrete time Fourier transform that reveals no differences between the original and reconstructed signal.

However, there are still issues with the nature of periodic extension. Due to sampling, the number of frequency components in the reconstructed signal is limited to *NFFT*. But even with a finite frequency resolution, no matter how

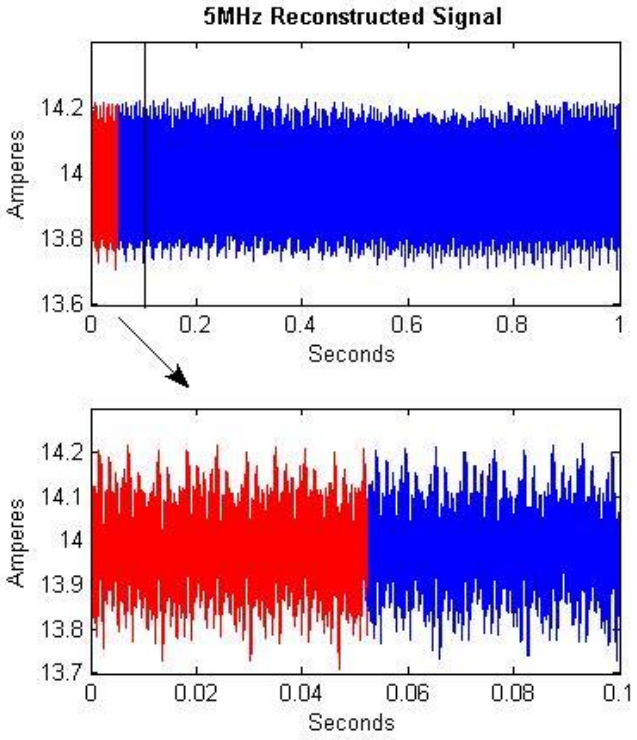

Fig. 2. The original inverter noise waveform (red) is extended to a full one-second duration (blue) using IFFT reconstruction. The original signal length is now a power of 2.

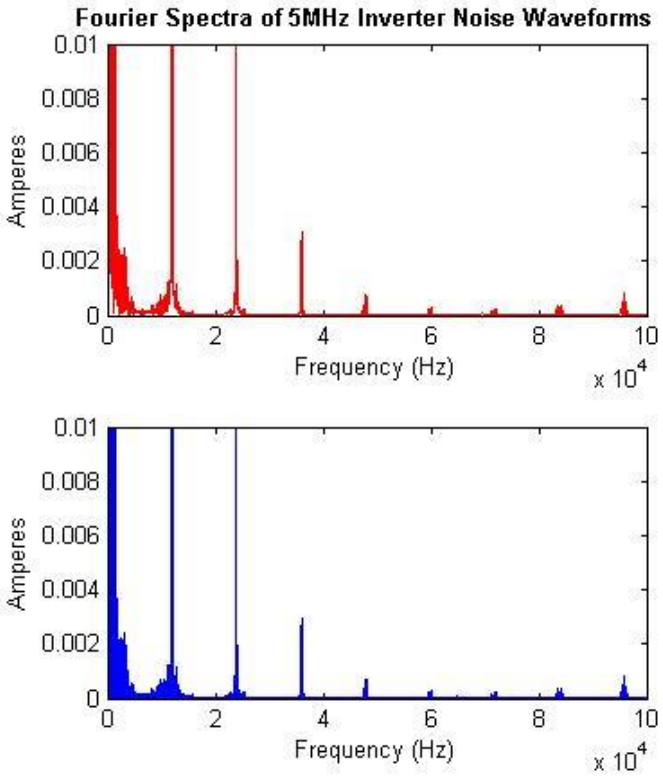

Fig. 3. The original 5MHz inverter noise spectrum (red) appears the same as the spectrum of the extended one-second duration waveform (blue) as shown in the range from 0 to 100kHz.

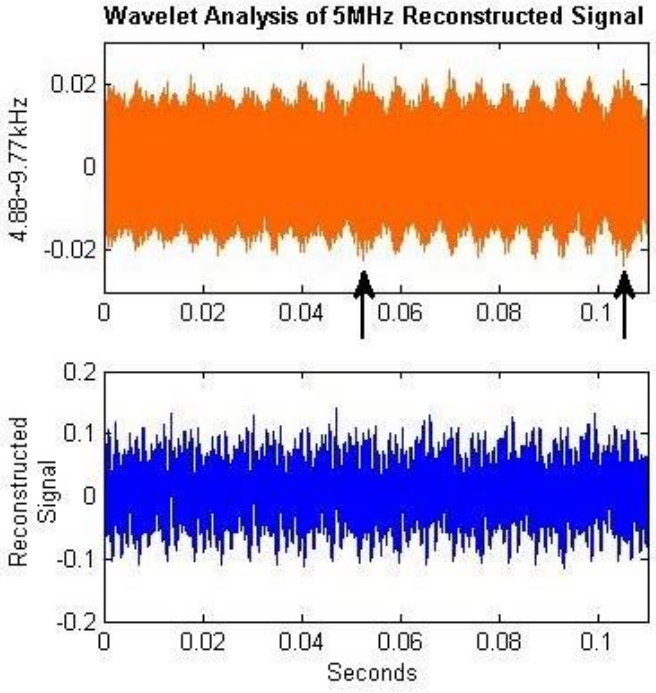

Fig. 4. Wavelet decomposition in the range of 4.88~9.77kHz (orange) highlights otherwise imperceptible changes in the frequency content of the reconstructed signal (blue).

the window is selected, it is in most cases impossible to satisfy the requirement that all frequency components have an integer number of periods within the FFT window. A wavelet decomposition analysis shown in Fig. 4 illustrates the effect of non-compliance with this requirement.

While the reconstructed 5MHz time-domain signal appears naturally continuous at multiples of the original signal length, the wavelet decomposition which keenly analyzes time-localized frequency content shows spikes at these points. Fig. 4 displays content relevant to the 4.88~9.77kHz band, but in fact the spike in frequency content is visible in nearly all sub-bands generated by wavelet transform at the multiples of the signal length, *N*. This spike in frequency content indicates an abrupt change in the time domain signal. Though it may be hard to visually discern in the time-domain with the high-frequency content present in the inverter noise, this may be connected with the onset of discontinuous periodic extension.

A complete solution to this problem only exists when the signal contains a least common multiple (LCM) of periods for all frequency components within the signal length, *N*. If the LCM > *N*, no appropriately sized window can be selected.

Therefore, testing conducted to determine the accuracy of arc detection methods relying on time-localized frequency content must be cognizant of and/or compensate for test signals extended through an IFFT-based method.

D. Growing the Dataset through Signal Extension

In summary, the process of time-domain signal extension has been demonstrated using an FFT and IFFT-based reconstruction technique. While the demonstration aimed to produce an extended 1-second test signal for a single inverter, this process may be repeated for any inverter noise signal of interest provided that imposing the power of two length and windowing requirements, i.e., reducing the signal length if necessary, does not diminish the frequency resolution or signal quality beyond levels needed for testing.

Building on this or other extension methods, a library of inverter noise signals should be assembled, extended, and replayed for sufficient durations for testing within practical limits of computational time and available memory.

III. Combining Noise with Arc

After extending the length of the test signal to the desired duration, the background noise data needs to be combined with arcing information to approximate real-world input for arc fault detectors in PV systems. For the authors' work, this is considered an approximation in part because of arcing data obtained through use of an arc fault generator, rather than finding and recording elusive "naturally occurring" arcs discovered within installed residential or commercial PV systems. More information regarding the production of the arc data can be found in [6].

Rather than combining the inverter noise data and synthetic arc signal using simple amplitude superposition, we can combine the signals at specific relative power magnitudes. Knowing the relative strength of one signal versus the other allows one to explore the limits and therefore the range of detectability. We define a concise arc-signal-to-noise ratio as follows:

$$ASNR = \frac{P_{arc}}{P_{noise}} \qquad (5)$$

An example of the composite arc signal plus inverter noise is illustrated in Fig. 5. A flow chart retracing the steps of the data combination process is depicted in Fig. 6.

With perhaps minor modifications to sampling rates, the composite synthetic waveform may be fed directly as an input into any digital arc fault detecting algorithm. A functional algorithm should be able to distinguish between the inverter noise and the superimposed arc, assuming that the detection method is based on time or frequency domain analysis. More robust methods will be capable of detecting the arc at lower ASNRs—ASNRs less than or equal to 0.01, for example, rather than the more obvious cases at ASNR levels greater than or equal to unity.

IV. Future Work

After the collection and digital processing of the inverter noise and arc fault signatures have been completed, these digital signals can be converted to the analog domain in order to test real world systems. A digital-to-analog converter that generates voltage and current waveforms followed by a power amplifier operating at true PV array power levels should be able to recreate waveforms from any of the stored test signals in the digital library. These high-power signals form the basis of a hardware test bench to evaluate the true capability of arc fault detection algorithms. If the microcontroller which houses a detection algorithm performs well in triggering arc

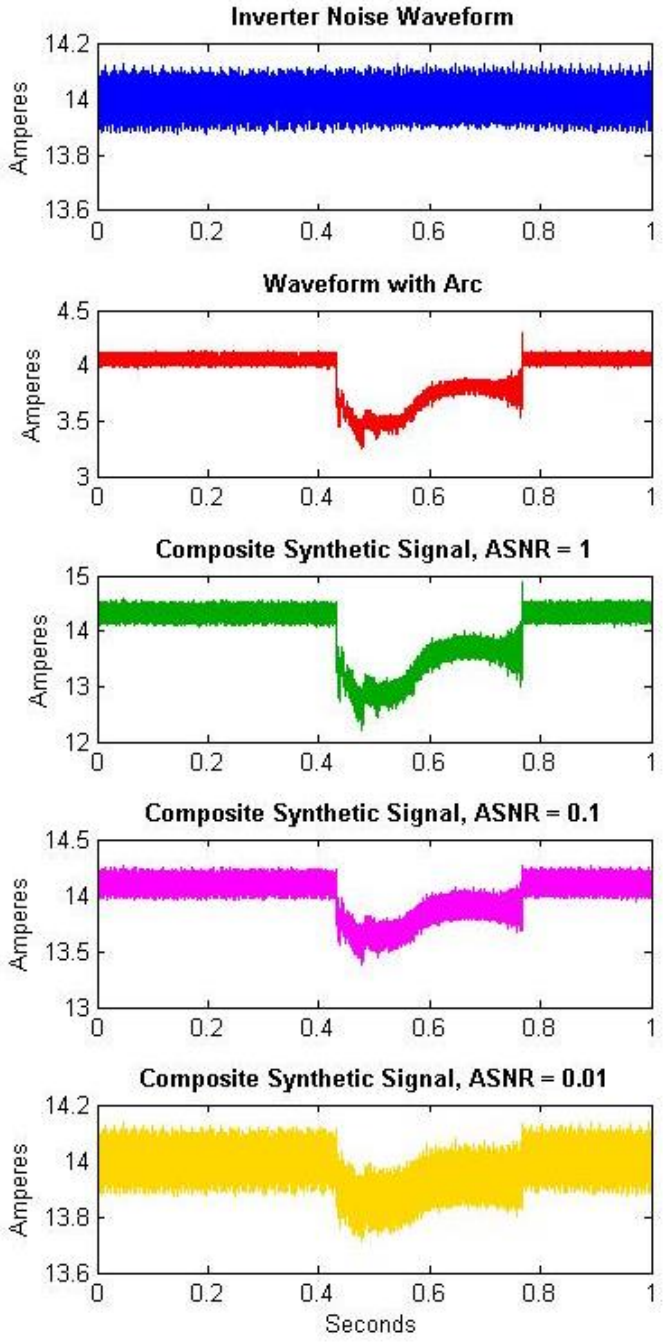

Fig. 5. The waveform with arc (red) is superimposed on the inverter noise waveform (blue) at ASNR = 1, 0.1 and 0.01 to produce the composite synthetic waveforms (green, magenta, and yellow).

fault circuit interrupters for the test bench, employing it for use in actual PV systems is the logical next-step and also the end goal of this work.

In Fig. 7 we see the envisioned setup of the hardware test bench. A laptop or desktop computer is used to process and prepare the test signal from the inverter noise library at the desired ASNR. After converting the test signal to the analog domain, the signal undergoes preliminary amplification to prepare it for subsequent coupling with a high DC-power solar array simulator. This signal is then fed to the device under test (DUT) which triggers the arc fault circuit interrupter (AFCI) upon detection of an arc.

This described system has the advantage that each of the steps and/or components within the system are modular and inexpensive in comparison with hardware testing that involves redirecting operations at a solar farm or installation of new PV arrays for testing purposes.

It also allows for repeatability in testing. Those who would conduct the tests do not need to rely on chance for appropriate weather and atmospheric conditions. The PV simulator output coupled with the high-frequency components from the conditioned test signal provide all necessary controls. The DC voltage and current can be specified as well as the power level of the inverter noise and embedded arc signal. Selecting and synthesizing new test signals from the inverter noise library allows the DUT to pass through multiple trials which each represent different possible PV installations without requiring reassembly or change of venue.

V. Conclusion

A method to ascertain the quality of arc fault detection algorithms has been discussed. Taking inverter noise measurements from actual PV systems provides essential data for use in the preparation of test signals. Extending test signals to sufficient length ensures verification of detection and gives alerts of false positives. FFT analysis followed by IFFT-based reconstruction provides one means of reaching the test signal length requirement, although choosing an appropriate window to satisfy a perfect reconstruction for all frequency components may be difficult.

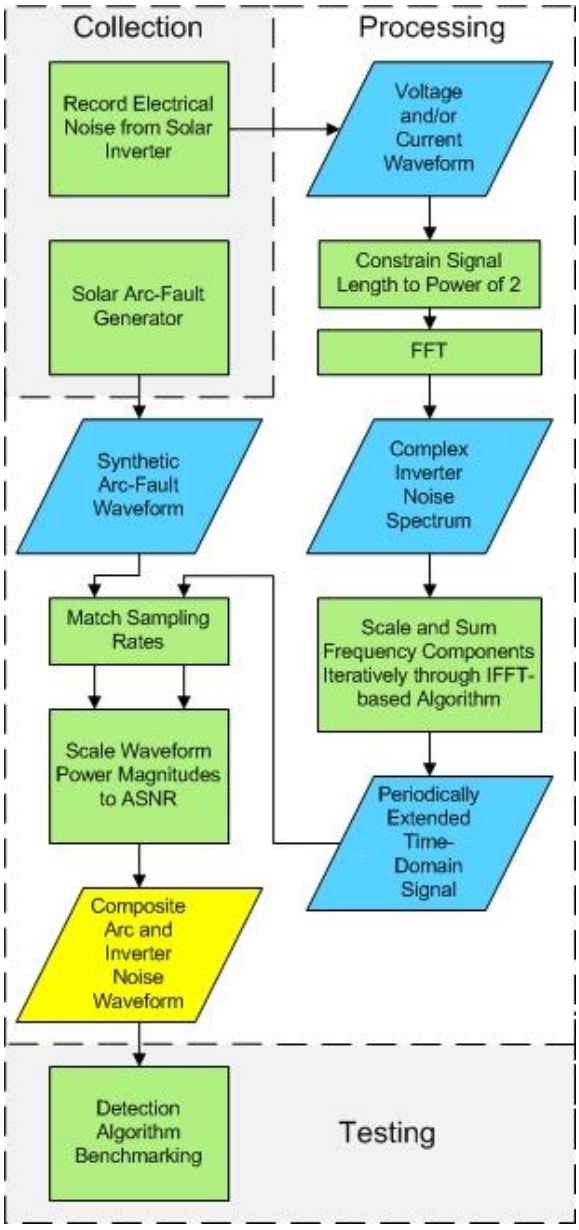

Fig. 6. Diagram following the data from the collection phase through processing until the composite arc and inverter noise waveform is ready for use in testing.

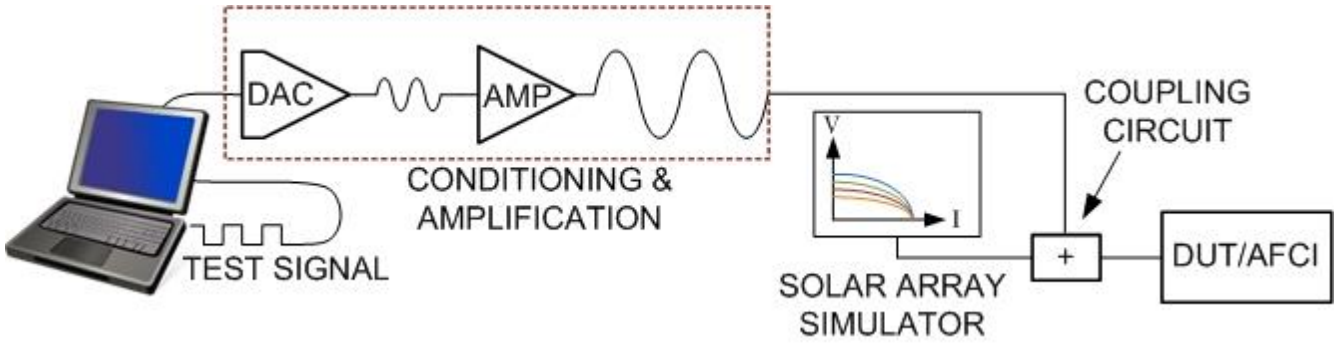

Fig. 7. A test signal produced by the computer passes through conditioning and amplification into a coupling circuit which combines high power DC with the high frequency test signal at the appropriate magnitude. The resulting signal serves as direct input for the DUT.

Defining an arc-signal-to-noise ratio further allows for specific quantification of arc detecting capability.

Future work involves implementing the digitally synthesized signals in the analog domain. A hardware test bench built on the inverter noise library according to the system described in Fig. 7 is capable of performing repeatable, controlled experiments on the devices that execute arc detection algorithms.

Following these proposed methods, industry and regulatory entities can utilize inverter noise field data in combination with synthetic arcing information to evaluate the quality of arc fault detectors. Ensuring accurate and robust detection algorithms in turn improves the reliability and safety of PV systems.

ACKNOWLEDGEMENT

This research was partially funded by the Department of Energy's Office of Energy Efficiency and Renewable Energy through a collaboration with Sandia National Laboratories. Sandia National Laboratories is a multi-program laboratory managed and operated by Sandia Corporation, a wholly owned subsidiary of Lockheed Martin Corporation, for the U.S. Department of Energy's National Nuclear Security Administration under contract DE-AC04-94AL85000.

REFERENCES

[1] J. Johnson, B. Pahl, C. Luebke, T. Pier, T. Miller, J. Strauch, *et al.*, "Photovoltaic DC Arc Fault Detector testing at Sandia National Laboratories," in *Photovoltaic Specialists Conference (PVSC), 2011 37th IEEE*, 2011, pp. 003614-003619.

[2] Y. Xiu, J. Shengchang, L. Herrera, and W. Jin, "DC Arc Fault: Characteristic Study and Fault Recognition," in *1st International Conference on Electric Power Equipment - Switching Technology (ICEPE-ST)*, 2011, pp. 387-390.

[3] C. Strobl and P. Meckler, "Arc Faults in Photovoltaic Systems," in *Electrical Contacts (HOLM), 2010 Proceedings of the 56th IEEE Holm Conference on*, ed, 2010, pp. 1-7.

[4] X. Zhou, J. J. Shea, J. C. Engel, K. L. Parker, and T. J. Miller, "Arc Fault Circuit Interrupter and Method of Parallel and Series Arc Fault Detection," U.S. Patent 7,558,033 B2, Jul. 7, 2007.

[5] A. V. Oppenheim and R. W. Schafer, *Discrete-Time Signal Processing*, 3rd ed. New York: Pearson, 2010, pp. 76.

[6] W. Zhan and R. S. Balog, "Arc fault and flash detection in DC photovoltaic arrays using wavelets," in *Photovoltaic Specialists Conference (PVSC), 2013 IEEE 39th*, 2013, pp. 1619-1624.